

# Correlation Properties in Channels with von Mises-Fisher Distribution of Scatterers

Kenan Turbic, *Member, IEEE*, Martin Kasparick, and Sławomir Stańczak, *Senior Member, IEEE*

**Abstract**—This letter presents simple analytical expressions for the spatial and temporal correlation functions in channels with von Mises-Fisher scattering. In contrast to previous results, the expressions presented here are exact and based only on elementary functions, clearly revealing the impact of the underlying scattering parameters. The derived results are validated by a comparison against numerical integration, where an exact match is observed. To demonstrate their utility, the presented results are used to analyze spatial correlation across different antenna array geometries and to investigate the temporal correlation of a fluctuating radar signal from a moving target.

**Index Terms**—Wireless communications, Radar, 3D scattering, von Mises-Fisher distribution, Spatial correlation.

## I. INTRODUCTION

THE von Mises-Fisher (vMF) distribution is a widely adopted statistical model for angular distribution of scatterers in wireless communication channels, e.g., [1], [2], taking both the azimuth and elevation aspects of propagating waves into account. The good fit to measurements and the ability to model non-isotropic scattering with different degrees of angular concentration of multipath components are its main advantages over the alternative models in the literature [3]. Due to its simplicity, the vMF distribution is preferred over more general models, such as the Fisher-Bingham (FB5) distribution [4].

While the vMF model is widely adopted, the associated statistics and the impact of the underlying parameters are not fully understood yet, primarily due to the lack of closed-form analytical results. The existing studies of spatial correlation characteristics are either based on numerical integration [3], employ spherical wave expansion involving expressions with infinite sums of spherical Bessel functions [5], or obtain approximate analytical solutions under restrictive assumptions [6]. While these studies have greatly contributed to the initial understanding of non-isotropic scattering channels, the provided expressions are cumbersome and prohibit analytical inference, or their applicability is very restricted.

In this letter we present simple closed-form expressions for spatial- and auto-correlation functions in vMF scattering

This work was partially supported by the Federal Ministry of Education and Research (BMBF, Germany) in the “Souverän. Digital. Vernetzt.” programme, joint Project 6G-RIC; project identification numbers: 16KISK020K and 16KISK030. It was developed within the scope of COST Action CA20120 (INTERACT). The associate editor coordinating the review of this paper and approving it for publication was XX. (*Corresponding author: Kenan Turbic*.)

The authors are with the Wireless Communications and Networks Department, Fraunhofer Institute for Telecommunications, Heinrich Hertz Institute (HHI), Berlin, 10587 Germany (e-mail: kenan.turbic@hhi.fraunhofer.de, martin.kasparick@hhi.fraunhofer.de, slawomir.stanczak@hhi.fraunhofer.de).

S. Stanczak is also with Technische Universität Berlin, Berlin, Germany.

channels. In contrast to previous results, the presented expressions involve only elementary functions and do not rely on any approximations. Their simplicity facilitates analysis and clearly reveals the impact of the vMF distribution parameters.

Following our earlier internal report on this work in [7], some similar derivation steps appear to be independently applied in [8], considering channels between unmanned aerial vehicles employing uniform linear antenna arrays. In contrast to this work, we present simple expressions applicable to arbitrary 3D antenna array geometries, identify the direct impact of vMF scattering parameters, recognize the classic result for isotropic scattering as a special case and demonstrate the utility of the derived expressions in different use cases. As a novel application of the vMF scattering model, we additionally employ it to represent radar targets and analyze the impact of the target size on the corresponding signal fluctuation dynamics.

The rest of this letter is structured as follows. Channel model is introduced in Section II, while Section III presents the derivation of the spatial and temporal correlation functions. In Section IV, the obtained results are validated and used to analyze spatial correlation across different antenna arrays and to investigate temporal correlation of a signal from a moving radar target. The paper is concluded in Section V.

## II. CHANNEL MODEL

With multipath propagation taking place between a static Transmitter (Tx) and a mobile Receiver (Rx), the wideband channel transfer function can be written as

$$H(\Delta\mathbf{r}, f) = \sum_{n=1}^N A_n e^{-j2\pi f\tau_0^n} e^{j\frac{2\pi}{\lambda}\hat{\mathbf{k}}_n^T \Delta\mathbf{r}} \quad (1)$$

where

$f$  frequency;  
 $\lambda$  corresponding wavelength;  
 $N$  number of multipath components;  
 $A_n$  their amplitudes;  
 $\tau_0^n$  initial propagation delays;  
 $\hat{\mathbf{k}}_n$  Direction of Arrival (DoA) unit vectors, i.e.

$$\hat{\mathbf{k}}_n = (\cos\phi_n \cos\psi_n, \sin\phi_n \cos\psi_n, \sin\psi_n)^T \quad (2)$$

$\phi_n$  Azimuth Angles of Arrivals (AAoAs);  
 $\psi_n$  Elevation Angles of Arrivals (EAoAs);  
 $\Delta\mathbf{r}$  antenna position relative to the reference point, e.g., position at the beginning of the channel observation;  
 $(\cdot)^T$  vector transpose operation.

For the convenience of the derivations in the following section, the channel evolution is considered as a function of the spatial displacement of the Rx relative to its arbitrary initial position. The more traditional representation, as a function of time, follows from the adopted Rx mobility model, providing the time-displacement mapping.

The multipath components are assumed to arrive at the Rx with similar amplitudes, none of them being dominant. According to the central limit theorem, the envelope of (1) exhibits Rayleigh distribution in this case. While this requires  $N \rightarrow \infty$  in the theoretical reference model, it was demonstrated that  $N \geq 10$  is practically sufficient [9].

Scattering is assumed to occur in the far field of the mobile antenna, such that planar wave propagation can be assumed. This further implies that the DoAs and amplitudes of the arriving multipaths can be assumed constant over the local areas, several tens or hundreds of wavelengths in size [10].

The initial propagation delays, due to apparently random propagation path lengths at the reference point ( $\Delta\mathbf{r} = 0$ ), result in random phase shifts of the components arriving at the Rx. In practice, the differences between the delays  $\tau_0^n$  are typically much larger than the period of the carrier [9]. Thereby, the corresponding initial phases observed at any given frequency can be modeled as uniform random variables, i.e.,  $\varphi_0^n \sim \mathcal{U}(0, 2\pi)$ , which is the standard approach for narrowband channels<sup>1</sup>.

The DoAs are modeled by the vMF distribution, with its Probability Density Function (PDF) given by [11]

$$p_{\phi\psi}(\phi, \psi) = \frac{\kappa \cos \psi}{4\pi \sinh \kappa} e^{\kappa [\cos \mu_\psi \cos \psi \cos(\phi - \mu_\phi) + \sin \mu_\psi \sin \psi]} \quad (3)$$

where

- $\mu_\phi$  mean AAoA;
- $\mu_\psi$  mean EAoA;
- $\kappa$  spread parameter.

The parameters  $\mu_\phi$  and  $\mu_\psi$  specify the main direction of concentrated scattering and  $\kappa$  specifies the degree of concentration. For  $\kappa = 0$ , the distribution becomes uniform over a unit sphere.

### III. SPATIAL AND TEMPORAL CORRELATION

#### A. Spatial Correlation Function

Spatial Correlation Function (SCF) of the complex baseband envelope, normalized to unit power, is obtained as<sup>2</sup> [9]

$$\hat{R}_{hh}(\mathbf{d}_\Delta) = \mathbb{E} \{ H^*(\Delta\mathbf{r}_1, f) H(\Delta\mathbf{r}_2, f) \} \quad (4)$$

$$= \mathbb{E} \left\{ e^{j \frac{2\pi}{\lambda} \hat{\mathbf{k}}_\mu^T \mathbf{d}_\Delta} \right\} \quad (5)$$

where

- $\mathbf{d}_\Delta$  spatial displacement vector, i.e.  $\mathbf{d}_\Delta = \Delta\mathbf{r}_2 - \Delta\mathbf{r}_1$ .

By using the PDF in (3), the expectation (5) becomes

$$\hat{R}_{hh}(\mathbf{d}_\Delta) = \frac{\kappa}{4\pi \sinh \kappa} \times \int_{-\pi/2}^{\pi/2} \left\{ \int_{-\pi}^{\pi} e^{(b_x \cos \phi + b_y \sin \phi) \cos \psi} d\phi \right\} e^{b_z \sin \psi} \cos \psi d\psi \quad (6)$$

<sup>1</sup>The transmission coefficient of a narrowband channel is obtained by evaluating the channel transfer function (1) at the considered carrier frequency.

<sup>2</sup>We should note that the SCF is frequency-dependent, as imposed by the presence of the wavelength  $\lambda$  in (5).

with

$$b_x = \kappa \cos \mu_\phi \cos \mu_\psi + j \frac{2\pi}{\lambda} d_\Delta^x \quad (7)$$

$$b_y = \kappa \sin \mu_\phi \cos \mu_\psi + j \frac{2\pi}{\lambda} d_\Delta^y \quad (8)$$

$$b_z = \kappa \sin \mu_\psi + j \frac{2\pi}{\lambda} d_\Delta^z \quad (9)$$

and  $d_\Delta^{x/y/z}$  are components of the displacement vector  $\mathbf{d}_\Delta$ .

Employing [12, Eq. 3.338.4] to solve the inner integral in the azimuth angle variable yields

$$\hat{R}_{hh}(\mathbf{d}_\Delta)$$

$$= \frac{1}{2} \frac{\kappa}{\sinh \kappa} \int_{-\pi/2}^{\pi/2} I_0 \left( \sqrt{b_x^2 + b_y^2} \cos \psi \right) e^{b_z \sin \psi} \cos \psi d\psi \quad (10)$$

by considering that  $\cos \psi \geq 0$  for  $|\psi| \leq \pi/2$ . From the relationship between the modified and the regular Bessel functions [12, Eq. 8.406.3], it follows

$$\hat{R}_{hh}(\mathbf{d}_\Delta)$$

$$= \frac{1}{2} \frac{\kappa}{\sinh \kappa} \int_{-\pi/2}^{\pi/2} J_0 \left( \sqrt{B} \cos \psi \right) e^{b_z \sin \psi} \cos \psi d\psi \quad (11)$$

with

$$B = \left( \frac{2\pi}{\lambda} \right)^2 \|\mathbf{d}_\Delta\|^2 - \kappa^2 \cos^2 \mu_\psi - j 2\kappa \cos \mu_\psi \hat{\mathbf{k}}_\mu^T \mathbf{d}_\Delta \quad (12)$$

where

$\hat{\mathbf{k}}_\mu$  mean DoA unit vector, i.e.

$$\hat{\mathbf{k}}_\mu = (\cos \mu_\phi \cos \mu_\psi, \sin \mu_\phi \cos \mu_\psi, \sin \mu_\psi)^T \quad (13)$$

With a simple substitution, this integral can be reduced to the form in [12, Eq. 6.616.5], to obtain

$$\hat{R}_{hh}(\mathbf{d}_\Delta) = \frac{\kappa}{\sinh \kappa} \frac{\sinh \sqrt{b_z^2 - B}}{\sqrt{b_z^2 - B}} \quad (14)$$

Finally, replacing (9) and (12) in (14), and employing [12, Eq. 1.311.2], after some manipulation, yields

$$\hat{R}_{hh}(\mathbf{d}_\Delta) = \frac{\kappa}{\sinh \kappa} \text{sinc} \left( \sqrt{\left( \frac{2\pi}{\lambda} \right)^2 \|\mathbf{d}_\Delta\|^2 - \kappa^2 - j \frac{4\pi\kappa}{\lambda} \hat{\mathbf{k}}_\mu^T \mathbf{d}_\Delta} \right) \quad (15)$$

As we observe, the SCF depends on both the displacement distance and the displacement direction relative to the mean DoA, with the dependence on the latter being controlled by the spread parameter  $\kappa$ . For  $\kappa = 0$ , the dependence on the displacement direction disappears<sup>3</sup> and the SCF reduces to the classical result for 3D isotropic scattering [13], i.e.

$$\hat{R}_{hh}(\mathbf{d}_\Delta) = \text{sinc} \left( \frac{2\pi}{\lambda} \|\mathbf{d}_\Delta\| \right) \quad (16)$$

The SCF is real in this case. However, the SCF in (15) is complex in general, with its real part corresponding to the auto-correlation of the quadrature components and the imaginary one to their cross-correlation [9].

<sup>3</sup>In the limit as  $\kappa \rightarrow 0$ , the normalization factor in front of the sinc function in (15) is equal to one, as can be shown by applying L'Hopital's rule. Formally, a continuous extension of the function (15) is considered for  $\kappa = 0$ .

### B. Auto-correlation Function

By considering the spatial displacement between positions of the mobile antenna along its motion path, with employment of an appropriate mobility model, the SCF in (15) yields Auto-Correlation Function (ACF). For a linear motion at a constant velocity, the displacement vector can be expressed as

$$\mathbf{d}_\Delta = \mathbf{v} \Delta t \quad (17)$$

where

- $\Delta t$  time offset between Rx signal samples;
- $\mathbf{v}$  mobile antenna velocity vector, i.e.

$$\mathbf{v} = v(\cos \phi_v \cos \psi_v, \sin \phi_v \cos \psi_v, \sin \psi_v)^T \quad (18)$$

- $v$  mobile antenna speed;
- $\phi_v$  motion direction azimuth;
- $\psi_v$  motion direction elevation.

Replacing (17) in (15) yields the ACF, i.e.

$$\hat{R}_{hh}(\Delta t) = \frac{\kappa}{\sinh \kappa} \operatorname{sinc} \left( \sqrt{(2\pi f_m \Delta t)^2 - \kappa^2 - j4\pi\kappa f_\mu \Delta t} \right) \quad (19)$$

where

- $f_m$  maximum Doppler frequency shift, i.e.,  $f_m = \|\mathbf{v}\|/\lambda$ ;
- $f_\mu$  Doppler shift for the mean DoA, i.e.,  $f_\mu = \hat{\mathbf{k}}_\mu^T \mathbf{v} / \lambda$ .

In addition to typical mobile communication scenarios with static scatterers considered in Section II, (19) also applies when the scattering cluster is the one being dynamic, with the Tx/Rx being static. This is the case in radar systems, where scattering from a moving target be represented by a vMF-distributed cluster of multipaths and (19) can be thereby used to analyze temporal correlation characteristics of the corresponding signal fluctuations at the radar Rx.

However, for the monostatic radar case, the Doppler frequencies in (19) should be multiplied by a factor of two, to account for the fact that propagation path lengths change twice as fast compared to the change in the radar-target distance [14].

### C. Multi-cluster Scattering

The results in (15) and (19) apply for a single cluster of vMF-distributed scatterers. However, their generalization to the multi-cluster scattering case typical for practical scenarios is straightforward. As initially derived for 2D von Mises scattering in [15], the SCF in channels with multiple vMF scattering clusters can be written as<sup>4</sup> [3]

$$\hat{R}_{hh}(\mathbf{d}_\Delta) = \sum_{k=1}^{N_c} \hat{\Omega}_k \hat{R}_{hh}^k(\mathbf{d}_\Delta; \hat{\mathbf{k}}_{\mu,k}, \kappa_k) \quad (20)$$

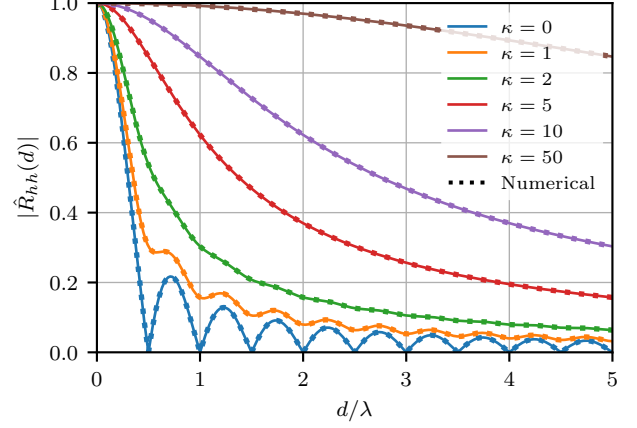
where

- $N_c$  number of scattering clusters;
- $\hat{\Omega}_k$  normalized power in the  $k$ -th cluster, i.e.,

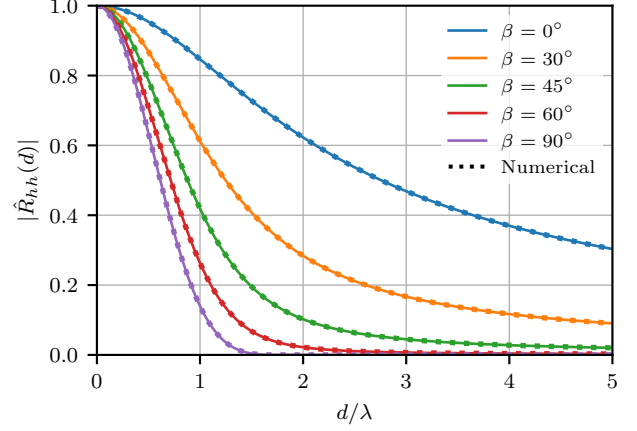
$$\sum_k \hat{\Omega}_k = 1 \quad (21)$$

$\hat{R}_{hh}^k$  SCF for the  $k$ -th cluster only, i.e., given by (15);

<sup>4</sup>Here we explicitly indicate the dependence on vMF scattering parameters, as they generally differ between clusters.



(a) Impact of the concentration parameter  $\kappa$  ( $\beta = 0^\circ$ ).



(b) Impact of displacement direction ( $\kappa = 10$ ), where  $\hat{\mathbf{k}}_\mu^T \mathbf{d}_\Delta = \|\mathbf{d}_\Delta\| \cos \beta$ .

Fig. 1. SCF in vMF scattering channels, showing the impacts of (a) the concentration parameter and (b) the direction of displacement; solid lines are obtained using (15) and the dotted ones via numerical integration.

$\kappa_k$  spread parameter for the  $k$ -th cluster;  
 $\hat{\mathbf{k}}_{\mu,k}$  mean DoA unit vector for the  $k$ -th cluster.

The ACF is obtained similarly, by replacing the SCFs for each cluster in (20) by the corresponding ACFs, i.e., given by (19).

## IV. RESULTS ANALYSIS

### A. Impact of vMF Distribution Parameters on SCF

The impact of vMF distribution parameters on spatial correlation is observed in Fig. 1, showing the SCF as a function of displacement distance,  $d = \|\mathbf{d}_\Delta\|$ , for different values of the concentration parameter  $\kappa$  (Fig. 1a) and for different relative angles  $\beta$  between the displacement direction and the mean DoA (Fig. 1b), where  $\hat{\mathbf{k}}_\mu^T \mathbf{d}_\Delta = \|\mathbf{d}_\Delta\| \cos \beta$ . Due to the parity of the cosine function, only the values of  $\beta \in [0^\circ, 90^\circ]$  need to be considered.

For  $\kappa = 0$ , the SCF is given by (16) and the characteristic oscillations of the sinc function are apparent in Fig. 1a. For higher values of  $\kappa$ , the SCF is complex and its magnitude falls off at a slower rate. Therefore, spatial correlation is higher more concentrated the scatterers are. The strong impact of the

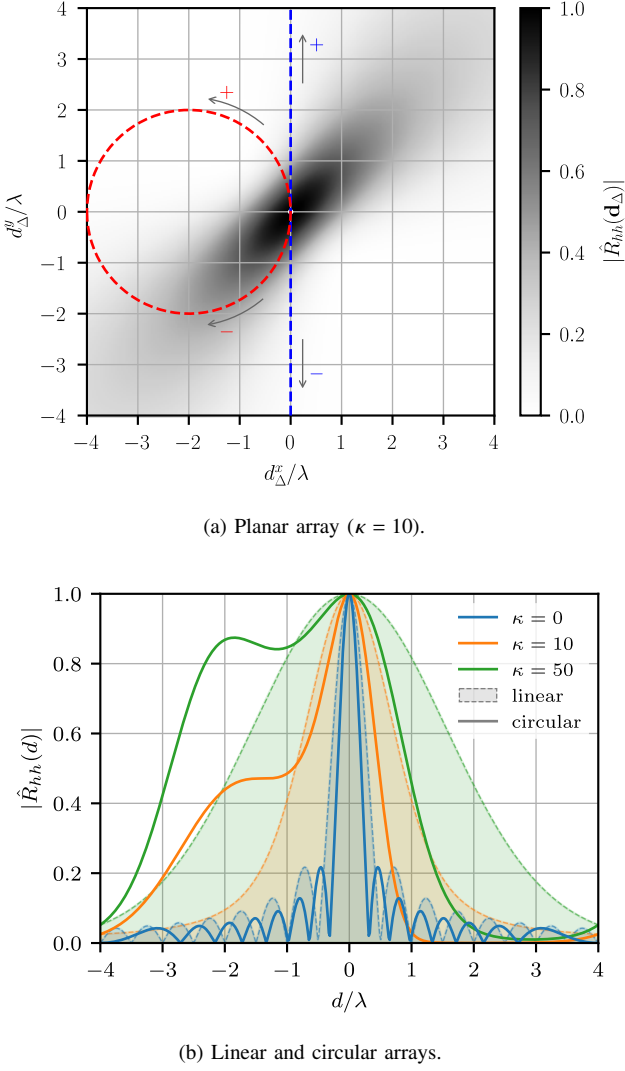


Fig. 2. SCFs for horizontal planar, linear and circular arrays; the array geometries corresponding to the results in (b) are outlined in (a).

displacement direction on the SCF is observed in Fig. 1b. The correlation is the highest for displacements in the direction of the mean DoA, and the lowest for the perpendicular direction.

To verify the correctness of the derived result in (15), Fig. 1 additionally shows SCF curves obtained via numerical integration (dotted lines). The exact match is observed in all cases, thereby validating the analytically derived results.

### B. Spatial Correlation over Antenna Arrays

Fig. 2 shows the SCF as a function of displacement distance over planar, linear and circular arrays in the horizontal plane, for vMF scattering with  $\mu_\phi = 45^\circ$  and  $\mu_\psi = 0^\circ$ . Fig. 2a shows the SCF across the surface of the horizontal planar array, i.e.,  $\mathbf{d}_\Delta = (d_\Delta^x, d_\Delta^y, 0)^T$ , with the dashed lines additionally indicating geometries of the considered linear (blue) and circular arrays (red). The reference point, relative to which the correlation is calculated, is indicated by the white dot in the origin. Fig. 2b shows the SCF curves obtained for displacements along the linear and circular array geometries in Fig. 2a.

One should note that the displacement vector along the linear array has a fixed orientation. On the other hand, its orientation is changing for points along the circular array. This means that the displacement distances on the horizontal axis in Fig. 2b are associated with different orientations of the displacement vector for the circular array case.

As observed in Fig. 2a for  $\kappa = 10$ , concentrated scattering results in a higher correlation over the planar array in the direction of the mean DoA projected onto the array surface. More concentrated scattering (higher  $\kappa$ ) results in a wider and more elongated area of increased spatial correlation in the direction of the mean DoA. On the other hand, for isotropic scattering ( $\kappa = 0$ ), the SCF is radially symmetric and exhibits variations according to the sinc function (16) in all directions.

In consistency with the previous observations, Fig. 2b shows that the signal de-correlates slower with the displacement along linear and circular arrays for more concentrated scattering. The SCF curves obtained for the linear array are symmetric (i.e., even) and thus stationary in spatial displacement distance along the array, with the parity of the SCF being preserved regardless of the array orientation. On the other hand, such a symmetry does not exist for the circular array and, in the considered case, a higher correlation is observed for the displacements in the negative direction, i.e., corresponding to the counter clockwise direction from the reference point along the circular path in Fig. 2a. Therefore, the SCF is generally non-stationary in spatial displacement along a circular array or, in general, for any non-linear one-dimensional array geometry.

### C. Temporal correlation of a fluctuating radar target

Fig. 3 shows the ACF of the Rx signal at a monostatic radar received for a target at an elevation angle of  $20^\circ$ , represented by a vMF-distributed cluster of scatterers, with size specified by its angular width,  $\Delta\theta$ . The velocity vector of the target is assumed to be constant, horizontal and pointing in the direction away from the radar. The operating frequency of the radar is assumed to be 10 GHz. The choice of the concentration parameter  $\kappa$  for a given  $\Delta\theta$  is detailed in Appendix A. To circumvent the numerical instability issues described in Appendix B, the approximation (23) is used to evaluate the SCF for the large values of  $\kappa$  in this scenario.

The results show that a faster moving target yields shorter signal de-correlation time. By considering samples with correlation below 0.5 as being uncorrelated, for the  $2^\circ$  angular target width the signal de-correlates nearly four times faster for target speed of 150 km/h (24 ms) than 40 km/h (85 ms). The target size also plays an important role, where the Rx signal de-correlates slower for smaller targets and faster for the larger ones. For the considered target speed of 150 km/h, the angular target widths of  $2^\circ$ ,  $1^\circ$  and  $0.5^\circ$  yield de-correlation times of 24 ms, 46 ms and 90 ms, respectively.

It is important to point out that the direction of target motion also has a significant impact on the Rx signal de-correlation which is not considered here, but can be anticipated based on the results in Fig. 1b. The Rx signal de-correlation with the change in the target's orientation is neglected here, but has an important impact in practical radar systems. Similarly, the

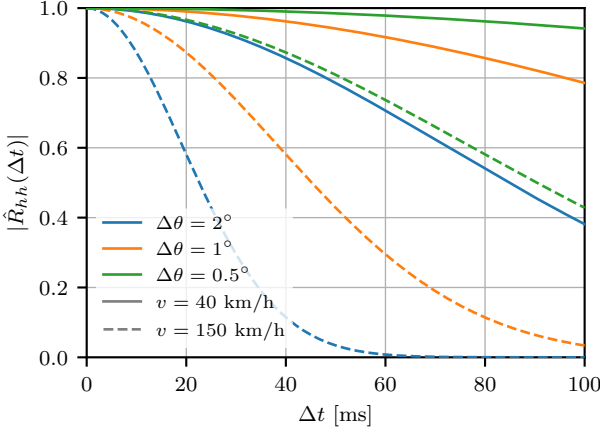


Fig. 3. ACF of the Rx radar signal from moving targets with different angular widths  $\Delta\theta$ , observed at  $20^\circ$  elevation while traveling at a constant altitude with speeds of 40 and 120 km/h, in azimuth direction away from the radar.

frequency correlation needs to be appropriately modelled in systems employing frequency agility techniques [14].

## V. CONCLUSIONS

The vMF distribution is a widely adopted model for representing clusters of scatterers in wireless communication channels, taking both the main direction and the concentration of scattering into account. This letter presents a simple closed-form expressions for the SCF and ACF in channels with vMF scattering. The simplicity of the presented expressions provides a better insight into the impact of the vMF distribution parameters on spatial correlation properties, and allows for analysis of arbitrary antenna array structures.

The correctness of the obtained expressions is verified by comparison against numerical integration results, where an exact match is observed. Together with the repeated experimental demonstration of the validity of the vMF scattering model in the literature, this agreement establishes practical relevance of the presented results.

To demonstrate their utility, the derived expressions are employed to analyze spatial correlation across planar, linear and circular arrays. The results show that concentrated scattering yields a higher spatial correlation in the direction of the mean DoA, increasing with higher values of  $\kappa$ . The non-stationarity of the SCF in displacement distance for circular and other non-linear array geometries is observed. The obtained results are also used to investigate temporal correlation characteristics of a radar signal reflected from a moving target, represented by a cluster of vMF-distributed scatterers, with the results showing the important impact of the target size, speed and motion direction on the Rx signal fluctuation dynamics.

## APPENDIX A

The value of  $\kappa$  corresponding to a given angular width of the target in Sec. IV-C is obtained according to

$$\kappa(\Delta\theta) = \frac{2}{1 - \cos\left(\frac{\Delta\theta}{2}\right)} \quad (22)$$

where

$$\Delta\theta \quad \text{angular width of the target seen by the radar.}$$

This expression is obtained by considering the angular deviation from the mean DoA, for which the vMF PDF falls to a fraction  $e^{-2} \approx 0.13$  of its maximum value.

## APPENDIX B

Due to the numerical instability of the available algorithms for evaluation of the sinh function for very large values of the argument, one encounters issues when using (15) to evaluate the SCF for very large  $\kappa$  (i.e., typically for  $\kappa > 700$ ). In this case, the following tight approximation is useful

$$\hat{R}_{hh}(\mathbf{d}_\Delta) \approx \kappa e^{-\kappa} \frac{e^{jz}}{jz} \quad (23)$$

where  $z$  is the argument of the SCF in (15), i.e.

$$z = \sqrt{\left(\frac{2\pi}{\lambda}\right)^2 \|\mathbf{d}_\Delta\|^2 - \kappa^2} - j \frac{4\pi\kappa}{\lambda} \mathbf{k}_\mu^T \mathbf{d}_\Delta \quad (24)$$

This approximation also applies to (19), with appropriately replaced argument  $z$ .

## REFERENCES

- [1] T. Wang, Y. Liu, M. Zhang, W. E. I. Sha, C. Ling, C. Li, and S. Wang, "Channel Measurement for Holographic MIMO: Benefits and Challenges of Spatial Oversampling," in *Proc. IEEE Int. Conf. Commun. (ICC)*, Rome, Italy, May 2023.
- [2] A. Pizzo, L. Sanguinetti, and T. L. Marzetta, "Spatial Characterization of Electromagnetic Random Channels," *IEEE Open J. Commun. Soc.*, vol. 3, pp. 847–866, Apr. 2022.
- [3] K. Mammasis, R. W. Stewart, and J. S. Thompson, "Spatial Fading Correlation model using mixtures of Von Mises Fisher distributions," *IEEE Trans. Wireless Commun.*, vol. 8, no. 4, pp. 2046–2055, Apr. 2009.
- [4] J. T. Kent, "The Fisher-Bingham Distribution on the Sphere," *J. R. Stat. Soc. B, Methodological*, vol. 44, no. 1, pp. 71–80, 1982.
- [5] K. Mammasis and R. W. Stewart, "Spherical Statistics and Spatial Correlation for Multielement Antenna Systems," *EURASIP J. Wireless Com. Network*, vol. 2010, no. 1, Dec. 2010.
- [6] Q. Zhu, Y. Yang, C.-X. Wang, Y. Tan, J. Sun, X. Chen, and W. Zhong, "Spatial Correlations of a 3-D Non-Stationary MIMO Channel Model With 3-D Antenna Arrays and 3-D Arbitrary Trajectories," *IEEE Wireless Commun. Lett.*, vol. 8, no. 2, pp. 512–515, Apr. 2019.
- [7] K. Turbic, M. Kasparick, and S. Stanczak, "Correlation Properties of Channels with von Mises-Fisher Scattering," COST Action CA20120 (INTERACT), Lisbon, Portugal, Technical Document TD(24)07079, Jan. 2024.
- [8] L. Zeng, X. Liao, Z. Ma, H. Jiang, and Z. Chen, "UAV-to-UAV MIMO Systems Under Multimodal Non-Isotropic Scattering: Geometrical Channel Modeling and Outage Performance Analysis," *IEEE Internet Things J.*, 2024, Early Access (April 30, 2024).
- [9] M. Pätzold, *Mobile Radio Channels*, 2nd ed. West Sussex, UK: John Wiley & Sons Ltd., 2012.
- [10] A. F. Molisch, *Wireless Communications*, 2nd ed. Chichester, UK: John Wiley & Sons, 2011.
- [11] K. V. Mardia and P. E. Jupp, *Directional Statistics*. Chichester, UK: John Wiley & Sons, 2000.
- [12] I. S. Gradshteyn and J. M. Ryschik, *Table of Integrals, Series, and Products*, 7th ed. San Diego, California, USA: Academic Press, 2007.
- [13] R. K. Cook, R. V. Waterhouse, R. D. Berendt, S. Edelman, and M. C. Thompson Jr., "Measurement of Correlation Coefficients in Reverberant Sound Fields," *J. Acoust. Soc. Am.*, vol. 27, pp. 1072–1077, Jun. 1955.
- [14] M. I. Skolnik, *Introduction to Radar Systems*, 3rd ed. New York, NY, USA: McGraw-Hill, 2001.
- [15] C. B. Ribeiro, E. Ollila, and K. Visa, "Propagation Parameter Estimation in MIMO Systems using Mixture of Angular Distributions Model," in *Proc. IEEE Int. Conf. Acoust., Speech, Signal Process. (ICASSP)*, Philadelphia, PA, USA, 2005.